# Quadruplets of exceptional points and bound states in the continuum in dielectric rings

N. S. Solodovchenko⬤

*School of Physics and Engineering, ITMO University, St. Petersburg 191002, Russia*

K. B. Samusev⬤ and M. F. Limonov[*]

*School of Physics and Engineering, ITMO University, St. Petersburg 191002, Russia*
*and Ioffe Institute, St. Petersburg 194021, Russia*

The photonic properties of a narrow dielectric ring with a rectangular cross section are studied analytically and numerically. It is shown that exceptional points in such a resonator exist in pairs, with each point adjacent in parametric space to a bound state in the continuum, resulting in the formation of quadruplets of singular photonic states. The appearance of quadruplets is determined by the interaction of two photonic branches, which can anticross or intersect in parametric space during the transition from the strong to weak coupling regime, which is described by the Friedrich-Wintgen model. A dielectric ring is an ideal object for modeling quadruplets due to the ability to arbitrarily change the shape of a rectangular cross section, that is, to accurately scan the areas of intersection of axial and radial Fabry-Pérot-like resonances along the height or width of the ring. The key role is played by the internal hole as an additional degree of freedom, which allows one to change the mode coupling coefficient and observe exceptional points. The regimes of electric field concentration inside a narrow dielectric ring at the incidence of a plane electromagnetic wave are also demonstrated. The discovery of quadruplets of singular photonic states is of fundamental importance for the development of the photonics of non-Hermitian structures. The proximity of the exceptional point and the high-$Q$ bound state in the continuum in parametric space allows easy switching between gain and loss regimes and opens up new perspectives for applications.

## I. INTRODUCTION

Our world is arranged in such a way that most systems are not closed, interact with each other, and are described by non-Hermitian physics. The non-Hermiticity provides rich topological properties that often have no analog in Hermitian structures. As a rule, a non-Hermitian eigenvalue problem does not have an orthogonal set of eigenvectors; moreover, eigenvectors can be collinear. A point in the parameter space at which non-Hermitian degeneracy is observed, i.e., at least two eigenvalues and eigenvectors coalesce, is called the exceptional point (EP) [1,2]. At EPs, two energy levels are connected by a square-root branch point; moreover, they are the values of one analytic function on two different Riemann eigenvalue sheets [3–13]. In this paper, we study the two-level problem, which is the simplest case of a non-Hermitian system. In general, EPs appear in various systems with spatially discrete or continuous degrees of freedom of multiple dimensionalities and also can be considered as a critical point, near which there is a transition from strong coupling to weak coupling [5]. If the system is described by more than two eigenvalue surfaces, then it is possible that more than two surfaces simultaneously collapse at the same point, creating a higher-order EP [14,15]. In particular, a third-order EP occurs when three eigenvalues simultaneously coalesce and the

square-root dependence of the eigenvalues around the exceptional point is replaced by a cube root.

For a narrow dielectric ring resonator (RR) with a rectangular cross section, the result of plotting the full dependence of both eigenvalues of the non-Hermitian Hamiltonian on structural parameters $(R_{out} - R_{in})/h$, $R_{in}/R_{out}$ demonstrates paired EPs, Figs. 1(b) and 1(c). For generality, when demonstrating the results we use the normalized size parameter $\alpha x = kR_{out}(1 - R_{in}/R_{out})$ where $k$ is the wave number. Paired EP generate a distinct double-Riemann-sheet topology in the complex band structure, which leads to bulk Fermi arcs [7].

EPs are observed in both quantum mechanical and classical problems. EPs are involved in quantum chaos and quantum phase transition, they produce impressive effects in a specific time dependence and multichannel scattering [5,8,12,16]. In various systems, isolated EPs in the parameter space [3,17–19] and continuous rings of EPs in the momentum space [20] were previously studied. In optics, active or passive systems with EPs exhibit various exotic properties, such as strong magnetoelectric response, being easily controlled by symmetry-breaking perturbations [21], laser mode selection [22], sensor sensitivity enhancement [23], electromagnetically induced transparency at a chiral EP [24], mode switching [17], directional omnipolarizer [25], directional total absorption [26], and enhancement of Sagnac sensitivity [27] have been proposed and/or demonstrated.

EPs are closely related to the phenomenon of level repulsion [2], which has been originally explored in the context
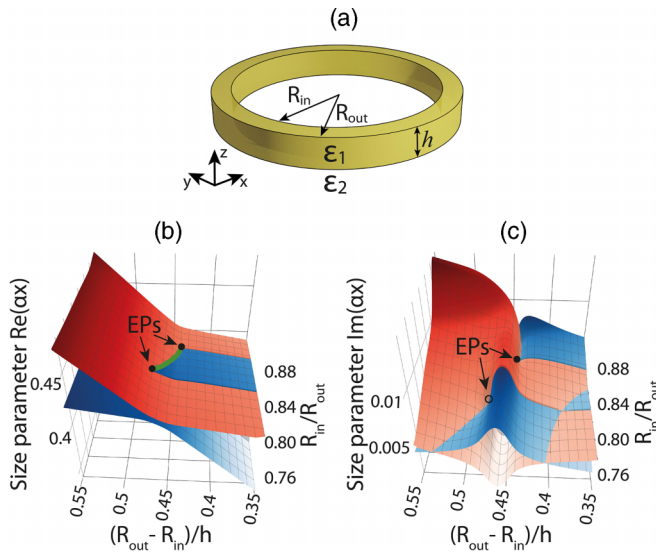
[*]m.limonov@metalab.ifmo.ru

FIG. 1. Exceptional points and bound states in the continuum in dielectric ring. (a) Ring parameters are $(R_{out} - R_{in})/h = 0.472$, $R_{in}/R_{out} = 0.8005$, $\varepsilon_1 = 80$, the ring is placed in a vacuum, ($\varepsilon_2 = 1$). (b), (c) Perspective view of the complex square-root topology of calculated eigenvalue surfaces $\text{Re}(\alpha x)$ and $\text{Im}(\alpha x)$ with a branch point singularity at two EP in the parameter space $(R_{out} - R_{in})/h$, $R_{in}/R_{out}$. In (b) two EPs are connected by a Fermi arc (green line). In (c) one of the EPs is hidden in this perspective by the bend of the Riemann sheet and depicted by a ring.

of quantum chaos [28]. In photonics, level repulsion is of interest because it indicates strong coupling and hybridization between states and typically occurs near an exceptional point in the real or complex parameter space [8]. One of the manifestations of level repulsion is associated with bound states in the continuum (BIC) that arise in accordance with the Friedrich-Wintgen model [29]. The history of BICs begins with the work of von Neumann and Wigner [30], who mathematically modeled a quantum system that has bound states above the continuum threshold. After almost 60 years, it was demonstrated that a similar phenomenon occurs in Maxwell's theory [31], after which the number of publications on this topic has continuously increased. BIC with an infinite quality factor is a mathematical model, and in real structures of finite sizes, quasi-BIC (qBIC) with a large but finite $Q$ factor is studied both theoretically and experimentally. The Friedrich-Wintgen's qBIC occurs when two nonorthogonal modes are coupled to the same radiation channel, interfere in the near field, and the avoided crossing arises in the parametric space [32–35]. Recently, the Friedrich-Wintgen model has been successfully utilized to interpret qBIC in dielectric cylinders [36] and rings [37,38]. For a single dielectric cylinder, qBIC occurs when two eigenmodes with different polarizations, associated with Mie-like resonances between the side walls and Fabry-Pérot-like resonances between the top and bottom walls of the cylinder, form an avoided crossing region in the strong coupling regime. These modes are approximately orthogonal inside the cylinder and interfere mainly in the near-field zone of the cylinder [15], realize qBIC, while the all-dielectric resonator demonstrates extremely high values of the $Q$ factor. In many cases the appearance of qBIC was accompanied by

the presence of the Fano resonance [31,36–38]. In particular, the link between the physics of Fano resonances [39,40] and qBICs excited in individual high-index dielectric nanoparticles has been experimentally demonstrated in Ref. [41].

Previously, we studied in detail the properties of qBIC during the transition from a homogeneous dielectric cylinder to a RR with a gradual increase in the diameter of the internal air cylinder to a value of $R_{in}/R_{out} = 0.6$ for $\varepsilon_1 = 80$ [37]. In that work, we analyzed the interaction of the $TE_{1,1,0}$ Mie-type mode and the $TM_{1,1,1}$ Fabry-Pérot-type mode. At $R_{in}/R_{out} \sim 0.53$, we found a crossover from the region of avoided crossing to the region of intersection of branches in the parametric space. In the region of intersection, the quasi-BIC is preserved and is observed in the spectra exclusively on the Mie-type $TE_{1,1,0}$ line, which is much narrower than the $TM_{1,1,1}$ line. Thus, in this case we do not observe an EP, since when the frequencies coincide, the half-widths of the lines differ.

The goal of the present work was to study the resonance properties of the RR by further expanding the internal hole to very thin rings. We were interested in the question of whether there are EPs in dielectric RRs and how they relate to qBICs. The behavior of a pair of resonant modes $TE_{0,2,0}$ and $TE_{0,1,2}$ in dielectric RRs forming qBIC according to the Friedrich-Wintgen model [29] was investigated, with the main attention being paid to the study of very narrow rings up to $R_{in}/R_{out} = 0.95$. As a result, we discovered that isolated clusters of singular photonic states exist in coordinate space. Such a cluster, which we called a quadruplet 2(EP + qBIC), is formed by two EPs connected by a Fermi arc and two qBICs, each of which is literally glued to one of the EP in coordinate space. We discovered two quadruplets in the parameter regions $R_{in}/R_{out} = 0.80–0.84$ and 0.9253–0.9308.

It should be noted that the existence of qBIC and EP in the same structure was noted earlier. The proximity of EP and BIC was also observed in a dielectric waveguide comprising a metal grating [42], in coupled polymer waveguides [43], in mirror-symmetry-broken metasurface [44]. However, we report 2(EP + qBIC) quadruplets, which may be of great interest for the development of non-Hermitian photonics.

## II. CALCULATION METHODS

Three methods were used to calculate the eigenvalues of a dielectric RR with a rectangular cross section: COMSOL MULTIPHYSICS, resonant state expansion (RSE), and temporal coupled-mode theory (TCMT).

The COMSOL MULTIPHYSICS program allows using the optical module to find eigenvalues (resonance frequencies) and eigenfunctions (electromagnetic field distributions), as well as the scattering cross section (SCS) $\sigma_{sca}$. In three-dimensional (3D) RRs the eigenfunctions can be characterized by the azimuthal ($m$), radial ($r$), and axial ($z$) mode indices, forming ordered triple ($m, r, z$). Since Maxwell's equations are scaled in the absence of dispersion, the defining geometric size (for example, the outer radius $R_{out}$) can be chosen arbitrarily. The inner radius of the RR varied over a wide range from $R_{in}/R_{out} = 0$ (cylinder) to $R_{in}/R_{out} = 0.95$ (narrow ring). The dielectric constant of the RR was chosen to be 80, when the resonance effects are most pronounced, which corresponds, for example, to high-index ceramics in the microwave range.

To calculate the eigenvalues and eigenfunctions in COMSOL, the eigenfrequency mode was used, while the resonator was surrounded by perfectly matched layer (PML), and the incident wave was absent. The scattering cross section was calculated only for one partial harmonic of the corresponding symmetry of the considered modes, $m = 0$. The scattering cross section $\sigma_{sca,0}$ was normalized to $S = 2R_{out}h$ (see Appendix A for more details).

Another approach to find the eigenvalues of the dielectric RR used in this work is RSE, which is an exact method of perturbation theory [45,46]. As a set of basis functions, we took the eigenvectors of a dielectric sphere with the same permittivity $\varepsilon_\alpha^{(0)}$ with frequencies $kR_{out,sphere} < 20$ and orbital angular momentum $l < 60$, which is sufficient for convergence of 99.5% of the real part of the frequency even for a narrow ring, geometrically distant from the sphere. The problem of finding the eigenvalues of the RR within the framework of this method is reduced to a matrix equation (see Appendix B), where the perturbation function changes the permittivity of the sphere, turning it into a ring, and the perturbation coefficients are found using the eigenfunctions of the sphere. Note that the problem is non-Hermitian due to the outgoing wave. Consequently, the eigenvectors grow exponentially at large distances, and their correct normalization deviates from the standard [45,46] (see Appendix B for more details).

The mechanism of the appearance of the Friedrich-Wingten's qBIC suggests that this effect is close to the appearance of EP. Indeed, in this case, qBICs arise as a result of the interaction of two eigenmodes of the structure, which can lead to level anticrossing, but, under certain structure parameters, can also lead to level crossing $Re_1(\alpha x) = Re_2(\alpha x)$, which, in general, corresponds to a transition from a strong coupling to a weak coupling regime [37]. However, an even more intriguing case is possible, when both real and imaginary parts of the eigenvalues coalesce, and an EP is achieved: $Re_1(\alpha x) = Re_2(\alpha x)$ and $Im_1(\alpha x) = Im_2(\alpha x)$. Therefore, all essential aspects of the Friedrich-Wingten's qBICs and EPs can be illustrated on an elementary level with the same two-level model. According to the temporal coupled-mode theory [1], when two resonances are eigenmodes of one resonator and are coupled to the same radiation channel, the amplitudes evolve with the Hamiltonian [2–5]:

$$H = \begin{pmatrix} \omega_1 & \kappa \\ \kappa & \omega_2 \end{pmatrix} - i \begin{pmatrix} \gamma_1 & \sqrt{\gamma_1\gamma_2} \\ \sqrt{\gamma_1\gamma_2} & \gamma_2 \end{pmatrix}. \qquad (1)$$

We consider the case when the two uncoupled resonances can have different resonance frequencies, $\omega_{1,2}$, and different radiative damping rates, $\gamma_{1,2}$. Here, $\kappa$ is the internal (near-field) coupling between the two resonators that radiate into the same channel, and therefore the interference of radiation gives rise to the via-the-continuum coupling term $\sqrt{\gamma_1\gamma_2}$. The condition for the occurrence of qBIC according to Friedrich-Wingten's model [29] has the form:

$$\kappa_{qBIC} = \frac{(\omega_1 - \omega_2)\sqrt{\gamma_1\gamma_2}}{(\gamma_1 - \gamma_2)}. \qquad (2)$$

Satisfying this condition, one can achieve a significant suppression of the total radiation losses of one of the modes. The resulting mode will be qBIC since it is formed according to the Friedrich-Wingten's mechanism, but some of the radiation

was not suppressed due to coupling with several radiation channels, which can be taken into account as an additional imaginary part to the coupling coefficient. As a result, the radical expression is extracted and we obtain expressions for two modes one of which is mostly real and becomes a qBIC.

The situation with the EP corresponds to the equality of the real and imaginary parts of the frequency. In contrast to the qBIC, the EP requires the setting of two parameters at once instead of one. Specifically, in the case of a ring, the parameters may be the height and radius of the inner hole. To observe the EP, two conditions must be met:

$$(\omega_1 - \omega_2) = -\frac{4\sqrt{\gamma_1\gamma_2}\,\kappa_{EP}}{(\gamma_1 - \gamma_2)} \qquad (3)$$

$$|\kappa_{EP}| = \pm(\gamma_1 - \gamma_2)/2. \qquad (4)$$

When $|\kappa| < |\gamma_1 - \gamma_2|/2$ corresponds to weak coupling and the modes intersect, and $|\kappa| > |\gamma_1 - \gamma_2|/2$ represents strong coupling and the modes anticross. Condition for $\kappa_{EP}$ resembles condition $\kappa_{qBIC}$ for the qBIC, but with inverted terms of the radiative damping rates, $\gamma_{1,2}$ and have different signs, so are observed on different sides with respect to the intersection of the real parts of the uncoupling modes.

In the case of interaction of two modes in a single dielectric resonator, described by Hamiltonian (1), EPs always appear in pairs, which is demonstrated by formula (4). Paired EPs [7,9,47] are connected in parameter space by an open arc, known as a bulk Fermi arc, along which the resonant frequencies of the two modes are degenerate [green line in Fig. 1(b)], but have different radiative damping rates, Fig. 1(c). Between two EP, the coupling coefficient is $|\kappa| < |\gamma_1 - \gamma_2|/2$. Using Hamiltonian (1) eigenvalue functions of COMSOL MULTIPHYSICS can be fitted and coupling coefficients can be defined (see Appendix C for more details).

When two noninteracting modes intersect, a qBIC can be obtained even if the near-field coupling coefficient $\kappa$ is zero, which is not the case for EP. The EP is observed only when conditions (3) and (4) are simultaneously satisfied and can be found in the space of two parameters. In connection with condition (4) for observing an EP, the near-field coupling coefficient $\kappa$ can have different signs, which forms a pair of EPs connected by a Fermi arc. Each EP corresponds to the neighboring qBIC, forming a quadruplet of singular points.

## III. RESULTS AND DISCUSSION: TWO QUADRUPLETS OF SINGULAR POINTS

Figure 2, which shows the calculated normalized scattering cross-section (SCS/$S$, $S = 2R_{out}h$) spectra of dielectric RRs in the spectral region of the $TE_{0,1,2}$ and $TE_{0,2,0}$ resonances. The results obtained make it possible to trace the emergence and transformation of both qBICs and EPs. For four fixed values of $R_{in}/R_{out}$, the SCS of the dielectric ring resonator ware calculated as a function of its aspect ratio $(R_{out} - R_{in})/h$ upon excitation by a plane TE-polarized wave. With this value, first, the resonance scattering spectra have narrow peaks that are convenient for treatment and interpretation.

We have previously demonstrated that in dielectric cylinders and rings there are two types of modes with different behavior depending on the aspect ratio $R_{out}/h$ [36,37]. Modes of the first type are formed mainly due to reflection from the
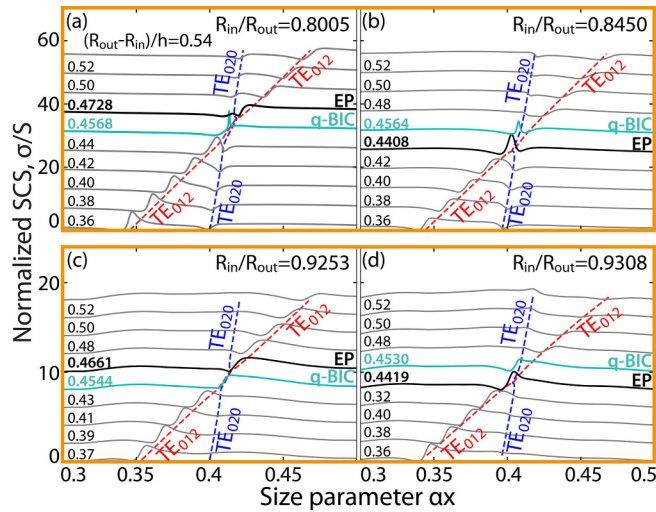
FIG. 2. Calculated spectra of the normalized SCS for dielectric RRs for two 2(EP + qBIC) quadruplets in yellow frames. The spectra are presented on the aspect ratio $(R_{out} - R_{in})/h$. The first quadruplet is shown in the top row, the second quadruplet in the bottom row, the Fabry-Perot-type $TE_{0,2,0}$ and Mie-type $TE_{0,1,2}$ modes interfere. SCS spectra are given in the range of $0.36 \leqslant R_{out}/h \leqslant 0.54$ with a step of 0.02. Curves are shifted vertically by 6 a.u. for $R_{in}/R_{out} = 0.8005$, 0.8450 and by 2 a.u. for $R_{in}/R_{out} = 0.9253$, 0.9308. The spectra highlighted with a thick black line correspond to EP, and the spectra highlighted with a thick purple line correspond to qBIC. Dotted lines are only a guide for the eyes. TE-polarized incident wave. $\varepsilon_1 = 80$, $\varepsilon_2 = 1$.



FIG. 3. Eigenvalues $\text{Re}(\alpha x)$ and $\text{Im}(\alpha x)$ for two 2(EP + qBIC) quadruplets, in yellow frames. Calculations for dielectric RRs with a rectangular cross section depending on the aspect ratio $(R_{out} - R_{in})/h$ and the parameter $R_{in}/R_{out}$, indicated at the top of (a), (c), (e), (g). (a)–(d) refer to the resonances of the first quadruplet, (e)–(h) to the resonances of the second quadruplet. (a), (c), (e), (g) Calculated real part of frequencies of the Fabry-Pérot-type $TE_{0,1,2}$ and the Mie-type $TE_{0,2,0}$ modes in qBIC and EP regimes as a function of the aspect ratio. (b), (d), (f), (h) Imaginary part of frequencies evolution demonstrating the presence of both qBIC and EP. The thin vertical dotted line indicates the position of the qBIC, and the thick line indicates the position of the EP. The green dashed lines indicate the symbolic Fermi arcs that connect EPs in the parametric space. The results of calculations by three methods: continuous curves, COMSOL; dotted lines, TCMT; circles, RSE. The dielectric permittivity of RRs is $\varepsilon_1 = 80$. The RRs are placed in the vacuum, $\varepsilon_2 = 1$.

side wall, are associated with the Mie resonances of an infinite cylinder, and, accordingly, have a slight frequency shift with a change in the length of the resonator. Modes of the second type are formed mainly due to reflection from two parallel faces of a cylinder or ring; they are similar to Fabry-Pérot modes and demonstrate a significant shift in the spectra with a change in the resonator length. Due to different spectral shifts, the $TE_{0,2,0}$ Mie-type and $TE_{0,1,2}$ Fabry-Pérot-type modes can have the same frequencies at some points in the parameter space, Fig. 2. Since the modes have the same azimuthal indices $m = 0$, they interact, and one of them turns into qBIC ($\gamma \to 0$), which is described by the Friedrich-Wintgen model [29]. The qBIC line in the scattering spectra can sharply narrow and, because of this, disappear both in the calculated and experimental spectra. In particular, the qBIC line in the calculated scattering spectra (COMSOL MULTIPHYSICS) on a dielectric cylinder with a permittivity $\varepsilon = 80$ was traced only up to a $Q$ factor of $10^4$ [48]. In the case of weak coupling, the lines corresponding to the $TE_{0,2,0}$ and $TE_{0,1,2}$ modes intersect in the scattering spectra, Fig. 2. At the same time, it turns out that in narrow dielectric RRs near the point where the qBIC appears, not only the real parts of the eigenvalues, but also the imaginary parts can coalesce [$\text{Re}_1(\alpha x) = \text{Re}_2(\alpha x)$, $\text{Im}_1(\alpha x) = \text{Im}_2(\alpha x)$], which leads to EPs that are formed in pairs, as follows from the analytical results (see Appendix C), and from numerical calculations, Fig. 1.

Figure 3 presents the main result of this work: the observation of two pairs of EPs, with each EP located in close proximity to another singular point, namely, to the qBIC.
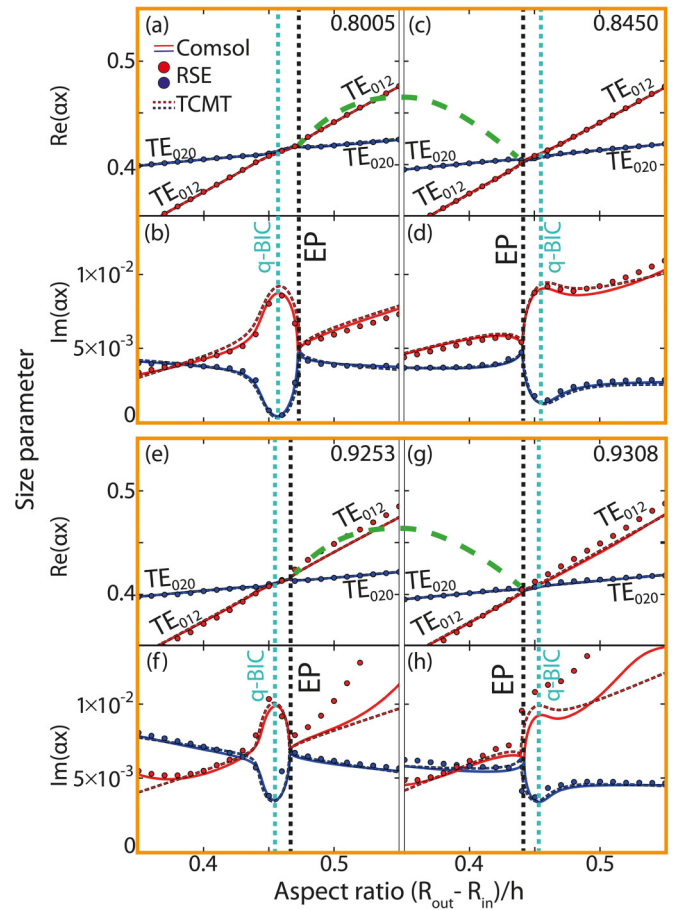
Indeed, at this singular point, the modes intersect, which means a weak coupling regime, however, in contrast to EP, one of the modes has a local maximum of the $Q$ factor, and the other a local minimum of the $Q$ factor. Thus, the pair EPs and the pair qBICs form a quadruplet 2(EP + qBIC) of connected singular points in the parametric space. In a very narrow dielectric ring, we found two quadruplets, and the singular points of the lower quadruplet in Figs. 3(e)–3(h) are especially close to each other, differing in the normalized width of the ring $R_{in}/R_{out}$ by only 0.0055.

It should be noted that the results obtained by three different methods are in good agreement. In particular, in many
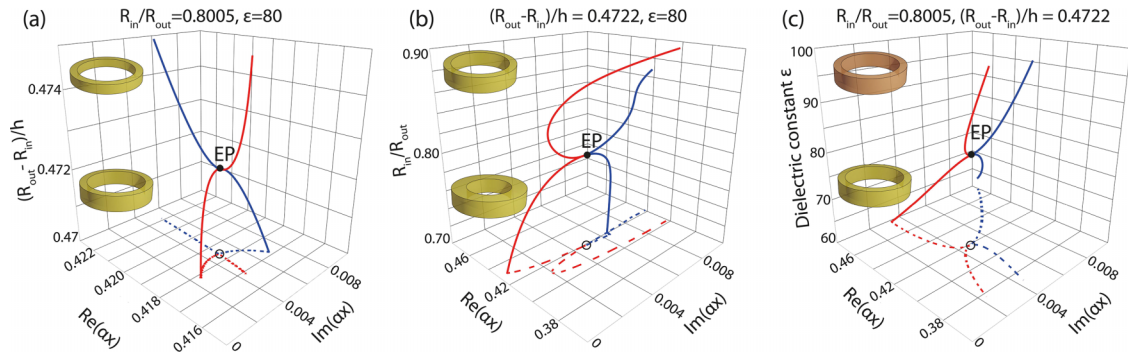
FIG. 4. Dispersion of the photonic branches of a dielectric RR with a rectangular cross section in the EP region. Dependences on the (a) height, (b) thickness, and (c) permittivity in the coordinate space $\mathrm{Re}(\alpha x)$, $\mathrm{Im}(\alpha x)$.

cases the results were so close that the lines in Fig. 3 completely coincided and the dotted line that represents the TCMT results becomes indistinguishable against the background of the solid lines representing the results of the calculations in COMSOL.

Figure 3 shows a significant analogy between the two quadruplets. In particular, a pair of singular points in quadruplets with a smaller $R_{\mathrm{in}}/R_{\mathrm{out}}$ parameter (0.8005 and 0.9253) is located in the qBIC-EP sequence in terms of aspect ratio $(R_{\mathrm{out}} - R_{\mathrm{in}})/h$, and a pair of singular points in quadruplets with a large $R_{\mathrm{in}}/R_{\mathrm{out}}$ (0.8450 and 0.9308) is located in the opposite sequence EP-qBIC.

However, there is also a difference between quadruplets, which is expressed in the form of a contour for the $\mathrm{TE}_{0,2,0}$ Mie-type resonance in the scattering spectra of two quadruplets. Figure 2 shows that in the spectra of the second quadruplet this resonance has an inverted line shape in the form of a dip, while the line of the first quadruplet is not inverted. The asymmetric line shape in such scattering spectra is determined by the Fano interference between narrow resonant lines and a broad background [39,40] (see Appendix D for more details).

The final Fig. 4 shows the dispersion of the photonic branches of a rectangular dielectric RR in the EP region with a change in three main parameters: normalized height [Fig. 4(a)], thickness [Fig. 4(b)], and permittivity [Fig. 4(c)] in the coordinate space $\mathrm{Re}(\alpha x)$, $\mathrm{Im}(\alpha x)$. The projections of branches are also shown on the plane $\mathrm{Re}(\alpha x)$, $\mathrm{Im}(\alpha x)$, which give an idea of the dispersion of branches in three-dimensional space. In particular, due to the projection in Fig. 4(a) it becomes clear that when the aspect ratio $(R_{\mathrm{out}} - R_{\mathrm{in}})/h$ changes at EP, both branches rotate 90 degrees. In this case, the rotation is not observed when the parameter $R_{\mathrm{in}}/R_{\mathrm{out}}$ and the permittivity $\varepsilon$ change, so the change in the height of the ring has the most dramatic effect on the character of the photonic system behavior of the dielectric ring in the EP.

## IV. CONCLUSIONS

In summary, in the spectra of dielectric rings, we theoretically discovered quadruplets of singular points formed by two EPs connected by a Fermi arc and two qBICs, each of which is adjacent to one of the EPs. The two 2(EP + qBIC) quadruplets were observed by three different methods, the results of which agree perfectly. The appearance of quadruplets

is determined by the interaction of two photonic branches, which can anticross or intersect in the parametric space during the transition from the strong to the weak coupling regime, which is described by the Friedrich-Wintgen's model. A dielectric ring is an ideal object for modeling quadruplets due to the ability to arbitrarily change the shape of a rectangular cross section, that is, to precisely scan the areas of intersection of axial and radial Fabry-Pérot-like resonances along the height or width of the ring. The key role is played by the internal hole as an additional degree of freedom, which allows one to change the mode-coupling coefficient and observe EPs. An important part of the work was the study of the electromagnetic field distribution in the ring and inside it. For EP and qBIC, the distributions have a characteristic form, which can be considered as photonic fingerprints of the corresponding resonances. We note the field in EPs, which corresponds to two zero-intensity cords inside the ring. Moreover, we have demonstrated the regimes of electric field concentration inside a narrow dielectric ring at the incidence of a plane electromagnetic wave.

The parity-time symmetry and non-Hermiticity opened up new ways of using gain, loss, and their coupling to control the light transport [9]. Our observation of pairs (EP + qBIC) will reveal the topological physics of bound states in the continuum in dielectric resonators in general, as well as create new optoelectronic devices based on resonant topological effects in dielectric rings, expanding the possibilities of sensing, filtering, switching, harmonic generation. The key point is the proximity of the EP and the high-$Q$ qBIC in the parametric space, which determines the possibility of easy switching between these resonances and resonantly increases the sensitivity and amplification of the system. Such a trigger mode can find application in further development of topological lasers [49–52] and non-Hermitian topological sensors [53]. Note that using the concept of parity-time symmetry to exploit the interplay between gain and loss, a microring laser has been demonstrated with resonant modes that can be controlled at will [22].

## APPENDIX A: SCATTERING SPECTRUM DECOMPOSITION IN TERMS OF AZIMUTHAL HARMONICS AND COMSOL SIMULATIONS

Determination of azimuthal harmonics is possible due to the decomposition of the total field **E**, **H** in terms of azimuthal harmonics.

$$\mathbf{E} = \sum_{m=-\infty}^{\infty} \mathbf{E}_m \exp(-im\phi),$$

$$\mathbf{H} = \sum_{m=-\infty}^{\infty} \mathbf{H}_m \exp(-im\phi). \tag{A1}$$

The total field is represented as the sum of the incident $\mathbf{E}_{\text{back}}$ and scattered $\mathbf{E}_{\text{sc}}$ fields. In case of zero azimuth harmonic, the incident field is a part of plane wave, the electric vector of which is perpendicular to the RR axis ($z$ axis), and the vector is directed along the $x$ axis (TE polarization). Such a field can be represented by the following equations:

$$E_\rho = -i\frac{E_0}{2}[J_1(k_x\rho) - J_{-1}(k_x\rho)]$$

$$E_\phi = -i\frac{E_0}{2}[J_1(k_x\rho) + J_{-1}(k_x\rho)]$$

$$E_z = 0, \tag{A2}$$

and the scattering cross section $\sigma_{\text{sca},0}$ of the zero harmonic will be the integral over the area of the remote sphere:

$$\sigma_{\text{sca},0} = \frac{c}{8\pi} \int_S \text{Re}(\mathbf{E}_{\text{sca},0} \times \mathbf{H}_{\text{sca},0})d\mathbf{S}/I_0. \tag{A3}$$

To calculate the structure, COMSOL uses 2D axisymmetric space, in which a geometric section of a ring surrounded by a PML layer is projected (Fig. 5). By specifying the explicit form of the incident field, one can solve the scattering problem. To calculate the scattering cross section, the energy of the scattered field is collected at the inner boundary of the PML. To calculate the eigenmodes, there was no annular incident field.

## APPENDIX B: RESONANT STATE EXPANSION

Another interesting and in this case theoretical method is resonant state expansion (RSE), which is an exact method of perturbation theory. RSE allows us to find the eigenvalues of the dielectric RR by perturbing the sphere. As a set of basis functions, we took the eigenvectors of a dielectric sphere with the same permittivity $\varepsilon_\alpha^{(0)}$ with frequencies $kR_{\text{out,sphere}} < 20$ and orbital angular momentum $l < 60$, which is sufficient for convergence of 99.5% of the real part of the frequency even for a narrow ring, geometrically distant from the sphere. The task of finding the eigenvalues of a RR within the framework
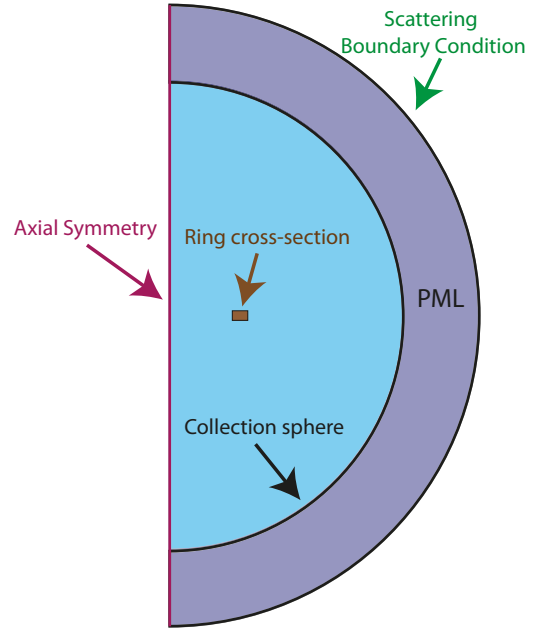


FIG. 5. Geometry of the problem for calculating the scattered field and eigenmodes.

of this method is reduced to a matrix equation of the form:

$$\frac{1}{\omega_\alpha} \sum_\beta (\delta_{\alpha\beta} + V_{\alpha\beta})b_\beta^j = \frac{1}{\Omega_j}b_\alpha^j, \tag{B1}$$

where $\omega_\alpha$ are the eigenfrequencies of a dielectric sphere with the same permittivity, $\Omega_j$ are the eigenvalues of the RR, and $V_{\alpha\beta}$ are the perturbation matrix elements, which are calculated by the formula:

$$V_{\alpha\beta} = \frac{1}{2} \int d\mathbf{r} \delta\varepsilon(\mathbf{r})\mathbf{E}_{rs}^\alpha(\mathbf{r})\mathbf{E}_{rs}^\beta(\mathbf{r}). \tag{B2}$$

Where $\delta\varepsilon$ is the perturbation function that changes the sphere into a ring resonator, and the fields $E_\alpha^{(0)}$ are the eigenvectors of the sphere. In general, $V$ is the transformation operator from a sphere to a ring. Note that the problem is non-Hermitian due to the outgoing wave. Consequently, the eigenvectors grow exponentially at large distances, and their correct normalization deviates from the standard.

## APPENDIX C: TEMPORAL COUPLED-MODE THEORY

In the general case, the Hamiltonian in the temporal coupled-mode theory has the following form (1):

$$H = \begin{pmatrix} \omega_1 & \kappa \\ \kappa & \omega_2 \end{pmatrix} - i\begin{pmatrix} \gamma_1 & \sqrt{\gamma_1\gamma_2} \\ \sqrt{\gamma_1\gamma_2} & \gamma_2 \end{pmatrix}.$$

We consider the case when the two uncoupled resonances can have different resonance frequencies, $\omega_{1,2}$, and different radiative damping rates, $\gamma_{1,2}$. Here, $\kappa$ is the internal (near-field) coupling between the two resonators that radiate into the same channel, and therefore the interference of radiation gives rise to the via-the-continuum coupling term $\sqrt{\gamma_1\gamma_2}$. The solution of this Hamiltonian can be found using the equality to zero of the determinant of this matrix. The solution can be written as

$$\widetilde{\omega}_{1,2} = \left(\frac{\omega_1 + \omega_2}{2} + i\frac{\gamma_1 + \gamma_2}{2}\right) \pm \frac{1}{2}\sqrt{[(\omega_1 - \omega_2)^2 + 4\kappa^2 - (\gamma_1 + \gamma_2)^2] + 2i[(\omega_1 - \omega_2)(\gamma_1 - \gamma_2) + 4\kappa\sqrt{\gamma_1\gamma_2}]}. \quad (C1)$$

By introducing additional notation

$$\omega_0 = \frac{\omega_1 + \omega_2}{2}; \quad \Omega = \omega_1 - \omega_2; \quad \gamma_s = \gamma_1 + \gamma_2; \quad \gamma_d = \gamma_1 - \gamma_2; \quad \gamma_0 = \sqrt{\gamma_1\gamma_2}, \quad (C2)$$

we can write in a more compact form:

$$\widetilde{\omega}_{1,2} = \left(\omega_0 + i\frac{\gamma_s}{2}\right) \pm \frac{1}{2}\sqrt{(\Omega^2 + 4\kappa^2 - \gamma_s^2) + 2i(\Omega\gamma_d + 4\kappa\gamma_0)} = \left(\omega_0 + i\frac{\gamma_s}{2}\right) \pm \frac{1}{2}\sqrt{a + ib}. \quad (C3)$$

This equation can be divided into real and imaginary parts:

$$\widetilde{\omega}_{1,2} = \left(\omega_0 \pm \frac{1}{2\sqrt{2}}\sqrt{a + \sqrt{a^2 + b^2}}\right) + i\frac{1}{2}\left(\gamma_s \pm \frac{\sqrt{2}\,b}{\sqrt{a + \sqrt{a^2 + b^2}}}\right). \quad (C4)$$

By examining the imaginary part of the roots as a function of $\Omega$, one can obtain the interaction parameter $\kappa_{\text{qBIC}} = (\omega_1 - \omega_2)\gamma_0/(\gamma_1 - \gamma_2)$ at which qBIC is observed. It follows from Eq. (C3) that when the real and imaginary parts of the expression standing under the root are equal to zero, two modes degenerate and form an EP. Equating the imaginary part of the equation standing under the root to zero gives condition (3). Substituting the obtained into the real part and also equating it to zero gives the relationship between the modulus of the interaction parameter and the modulus of the difference in damping rates (4):

$$(\omega_1 - \omega_2) = -\frac{4\sqrt{\gamma_1\gamma_2}\,\kappa_{\text{EP}}}{(\gamma_1 - \gamma_2)}$$

$$|\kappa_{\text{EP}}| = \pm(\gamma_1 - \gamma_2)/2.$$

Condition for $\kappa_{\text{EP}}$ resembles condition $\kappa_{\text{qBIC}}$ for the qBIC, but with inverted terms of the radiative damping rates, $\gamma_{1,2}$.
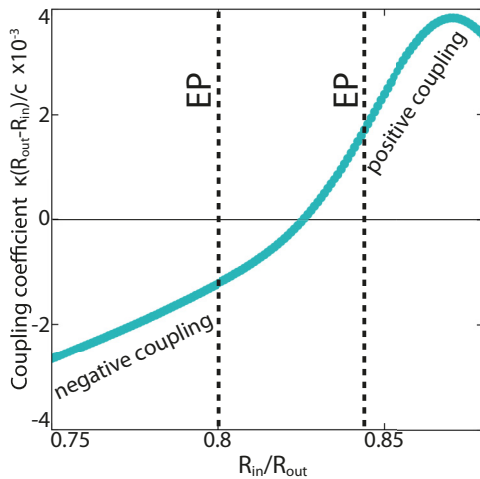


FIG. 6. The values of the coupling constant obtained for the first pair of EPs by fitting the eigenvalues by solving the Hamiltonian (1) as a function of the hole size $R_{\text{in}}/R_{\text{out}}$. A pair of EPs are illustrated with vertical dashed lines at $R_{\text{in}}/R_{\text{out}} = 0.8005$ and $0.8450$, respectively.

Using the obtained solution of the Hamiltonian, the dependences of the real $\text{Re}(\alpha x)$ and imaginary $\text{Im}(\alpha x)$ part of the normalized frequency of eigenmodes obtained in the COMSOL MULTIPHYSICS can be fitted. To do this, linear interpolations of the first and last points of solving the problem for eigenvalues with respect to the parameter $(R_{\text{out}} - R_{\text{in}})/h$ (COMSOL or RSE) can be taken as noninteracting modes. Using, for example, the least-squares method, one can obtain the interaction constant $\kappa$, where the data are the COMSOL MULTIPHYSICS solutions, and the function is the solution of the Hamiltonian (1). Figure 6 Shows that the EP pair is observed for different signs of the coupling constant at $R_{\text{in}}/R_{\text{out}} = 0.8005$ and $0.8450$, respectively, which corresponds to the formula $|\kappa_{\text{EP}}| = |\gamma_1 - \gamma_2|/2$. Since the formulas for $\kappa_{\text{EP}}$ and $\kappa_{\text{qBIC}}$ have different signs, they are observed on different sides with respect to the intersection of the real parts of the uncoupling modes.

## APPENDIX D: FANO RESONANCE

The Fano interference is described by the universal formula:

$$I(0) = D^2 \frac{(q + \Omega)^2}{1 + \Omega^2}, \quad (D1)$$

where $q = \cot\delta$ is the Fano asymmetry parameter, that determines the coupling of a narrow resonance with a continuum,



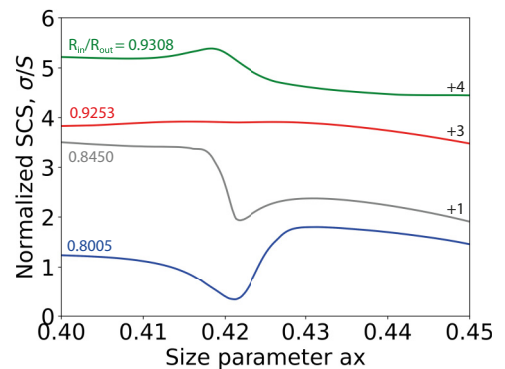FIG. 7. $\text{TE}_0 20$ resonance scattering spectrum at ratios supporting EPs. The spectra are shifted as indicated on the right.

$D^2 = 4\sin^2\delta$, $\delta$ is the phase difference between a narrow line and a broad line, $\Omega = (\omega - \omega_0)/(\gamma_0/2)$ is the dimensionless frequency, $\gamma_0$ and $\omega_0$ are the width and frequency of the narrow line. In the general case, the Fano profile has an asymmetric shape, which is determined by the parameter $q$, while we single out one limiting case of $q = 0$ when the Fano profile becomes a symmetric quasi-Lorentzian

antiresonance in the continuum spectrum $I(\omega) \sim \frac{\Omega^2}{1+\Omega^2}$, with the intensity $I(\omega) = 0$ at the eigenfrequency $\omega_0$. By changing the inner radius of the RR, one can change the Fano parameter and the amplitude of the resonance, which is clearly seen in Fig. 7. It can be seen that for $(R_{in}/R_{out})/h = 0.54$ the Fano parameters for $R_{in}/R_{out} = 0.8450$ and $0.9308$ are similar.

[1] T. Katō, *Perturbation Theory for Linear Operators* (Springer, Berlin, 1995), p. 619.

[2] W. D. Heiss, Phys. Rev. E **61**, 929 (2000).

[3] C. Dembowski, H.-D. Gräf, H. L. Harney, A. Heine, W. D. Heiss, H. Rehfeld, and A. Richter, Phys. Rev. Lett. **86**, 787 (2001).

[4] W. D. Heiss, J. Phys. A: Math. Theor. **45**, 444016 (2012).

[5] H. Cao and J. Wiersig, Rev. Mod. Phys. **87**, 61 (2015).

[6] K. Ding, G. Ma, M. Xiao, Z. Q. Zhang, and C. T. Chan, Phys. Rev. X **6**, 021007 (2016).

[7] H. Zhou, C. Peng, Y. Yoon, C. W. Hsu, K. A. Nelson, L. Fu, J. D. Joannopoulos, M. Soljačić, and B. Zhen, Science **359**, 1009 (2018).

[8] M.-A. Miri and A. Alù, Science **363**, aar7709 (2019).

[9] Ş. K. Özdemir, S. Rotter, F. Nori, and L. Yang, Nat. Mater. **18**, 783 (2019).

[10] R. El-Ganainy, K. G. Makris, M. Khajavikhan, Z. H. Musslimani, S. Rotter, and D. N. Christodoulides, Nature Phys. **14**, 11 (2018).

[11] M. Parto, Y. G. N. Liu, B. Bahari, M. Khajavikhan, and D. N. Christodoulides, Nanophotonics **10**, 403 (2020).

[12] E. J. Bergholtz, J. C. Budich, and F. K. Kunst, Rev. Mod. Phys. **93**, 015005 (2021).

[13] M. Masharin, A. Samusev, A. Bogdanov, I. Iorsh, H. Demir, and S. Makarov, Adv. Funct. Mater. **33**, 2215007 (2023).

[14] E. M. Graefe, U. Günther, H. J. Korsch, and A. E. Niederle, J. Phys. A: Math. Theor. **41**, 255206 (2008).

[15] K. Matsushima, Y. Noguchi, and T. Yamada, Phys. Rev. B **107**, 144104 (2023).

[16] H. A. Haus, *Waves and Fields in Optoelectronics* (Prentice-Hall, Hoboken, 1984), p. 402.

[17] W. Liu, Y. Zhang, Z. Deng, J. Ye, K. Wang, B. Wang, D. Gao, and P. Lu, Laser Photonics Rev. **16**, 202100675 (2022).

[18] H. Xu, D. Mason, L. Jiang, and J. G. E. Harris, Nature (London) **537**, 80 (2016).

[19] K. Kawabata, T. Bessho, and M. Sato, Phys. Rev. Lett. **123**, 066405 (2019).

[20] B. Zhen, C. W. Hsu, Y. Igarashi, L. Lu, I. Kaminer, A. Pick, S.-L. Chua, J. D. Joannopoulos, and M. Soljačić, Nature (London) **525**, 354 (2015).

[21] A. C. Valero, V. Bobrovs, D. Redka, A. S. Shalin, and Y. Kivshar, arXiv:2205.05735.

[22] H. Hodaei, M.-A. Miri, M. Heinrich, D. N. Christodoulides, and M. Khajavikhan, Science **346**, 975 (2014).

[23] Z. Liao, X. Peng, L. Liu, Y. Xu, K.-D. Xu, B. Pan, G. Q. Luo, and Y. Liu, Laser Photonics Rev. **17**, 00276 (2023).

[24] C. Wang, X. Jiang, G. Zhao, M. Zhang, C. W. Hsu, B. Peng, A. D. Stone, L. Jiang, and L. Yang, Nature Phys. **16**, 334 (2020).

[25] A. U. Hassan, B. Zhen, M. Soljačić, M. Khajavikhan, and D. N. Christodoulides, Phys. Rev. Lett. **118**, 093002 (2017).

[26] Y. Huang, C. Min, and G. Veronis, Opt. Express **24**, 22219 (2016).

[27] Y.-H. Lai, Y.-K. Lu, M.-G. Suh, Z. Yuan, and K. Vahala, Nature (London) **576**, 65 (2019).

[28] H.-J. Stockmann, *Quantum Chaos* (Cambridge University Press, Cambridge, 2006), p. 368.

[29] H. Friedrich and D. Wintgen, Phys. Rev. A **32**, 3231 (1985).

[30] J. von Neuman and E. Wigner, Phys. Z. **30**, 467 (1929).

[31] D. C. Marinica, A. G. Borisov, and S. V. Shabanov, Phys. Rev. Lett. **100**, 183902 (2008).

[32] H. M. Doeleman, F. Monticone, W. den Hollander, A. Alù, and A. F. Koenderink, Nature Photon. **12**, 397 (2018).

[33] S. I. Azzam, V. M. Shalaev, A. Boltasseva, and A. V. Kildishev, Phys. Rev. Lett. **121**, 253901 (2018).

[34] E. N. Bulgakov and D. N. Maksimov, Phys. Rev. A **98**, 053840 (2018).

[35] M. Odit, K. Koshelev, S. Gladyshev, K. Ladutenko, Y. Kivshar, and A. Bogdanov, Adv. Mater. **33**, 2003804 (2021).

[36] A. A. Bogdanov, K. L. Koshelev, P. V. Kapitanova, M. V. Rybin, S. A. Gladyshev, Z. F. Sadrieva, K. B. Samusev, Y. S. Kivshar, and M. F. Limonov, Adv. Photon. **1**, 1 (2019).

[37] N. Solodovchenko, K. Samusev, D. Bochek, and M. Limonov, Nanophoton. **10**, 4347 (2021).

[38] D. V. Bochek, N. S. Solodovchenko, D. A. Yavsin, A. B. Pevtsov, K. B. Samusev, and M. F. Limonov, Phys. Rev. B **105**, 165425 (2022).

[39] M. F. Limonov, M. V. Rybin, A. N. Poddubny, and Y. S. Kivshar, Nature Photon. **11**, 543 (2017).

[40] M. F. Limonov, Adv. Opt. Photonics **13**, 703 (2021).

[41] E. Melik-Gaykazyan, K. Koshelev, J.-H. Choi, S. S. Kruk, A. Bogdanov, H.-G. Park, and Y. Kivshar, Nano Lett. **21**, 1765 (2021).

[42] R. Kikkawa, M. Nishida, and Y. Kadoya, New J. Phys. **22**, 073029 (2020).

[43] H. Qin, X. Shi, and H. Ou, Nanophoton. **11**, 4909 (2022).

[44] Z. Zhou, B. Jia, N. Wang, X. Wang, and Y. Li, Phys. Rev. Lett. **130**, 116101 (2023).

[45] E. A. Muljarov, W. Langbein, and R. Zimmermann, Europhys. Lett. **92**, 50010 (2010).

[46] S. V. Lobanov, W. Langbein, and E. A. Muljarov, Phys. Rev. A **100**, 063811 (2019).

[47] C.-H. Yi, J. Kullig, and J. Wiersig, Phys. Rev. Lett. **120**, 093902 (2018).

[48] M. V. Rybin, K. L. Koshelev, Z. F. Sadrieva, K. B. Samusev, A. A. Bogdanov, M. F. Limonov, and Y. S. Kivshar, Phys. Rev. Lett. **119**, 243901 (2017).

[49] M. Brandstetter, M. Liertzer, C. Deutsch, P. Klang, J. Schöberl, H. E. Türeci, G. Strasser, K. Unterrainer, and S. Rotter, Nature Commun. **5**, 4034 (2014).

[50] B. Peng, Ş. K. Özdemir, S. Rotter, H. Yilmaz, M. Liertzer, F. Monifi, C. M. Bender, F. Nori, and L. Yang, Science **346**, 328 (2014).

[51] P. St-Jean, V. Goblot, E. Galopin, A. Lemaître, T. Ozawa, L. L. Gratiet, I. Sagnes, J. Bloch, and A. Amo, Nature Photon. **11**, 651 (2017).

[52] H. Zhao, P. Miao, M. H. Teimourpour, S. Malzard, R. El-Ganainy, H. Schomerus, and L. Feng, Nature Commun. **9**, 981 (2018).

[53] J. C. Budich and E. J. Bergholtz, Phys. Rev. Lett. **125**, 180403 (2020).